A distance and bandwidth dependent adaptive modulation scheme for THz communications

Alexandros-Apostolos A. Boulogeorgos*, Evangelos N. Papasotiriou*, and Angeliki Alexiou*
*Department of Digital Systems, University of Piraeus, Piraeus 18534, Greece. E-mails: al.boulogeorgos@ieee.org,{vangpapasot, alexiou }@unipi.gr

***Abstract*—In this paper, we provide a novel distance and frequency dependent adaptive modulation scheme, which is suitable for communication systems operating in the terahertz (THz) band. After determining the transmission bandwidth, the proposed scheme evaluates the subcarrier bandwidth of the orthogonal frequency division modulated (OFDM) transmission signal, in order to countermeasure the frequency selectivity of the THz channel. Next, the power is allocated to the OFDM subcarriers and the modulation order of the quadrature modulated (QAM) symbol loaded in each subcarrier is selected, based on the instantaneous channel conditions and a predetermined bit error rate (BER) requirement. The proposed link adaptation algorithm has low computational complexity and can significantly increase the link's throughput.**

I. Introduction

The increased data rates demand, in the beyond fifth generation (5G) wireless systems, as well as the fact that the spectral efficiency of the microwave links is approaching its fundamental limits have motivated the exploitation of higher frequency bands that offer interference-free and abundance of communication bandwidth [1]–[4]. Towards this end, THz band wireless communications have been recognized as an attractive canditate for providing an order of magnitude capacity improvements [5]–[7].

Although, THz systems can benefit from an extreme increase in the bandwidth, it comes at the price of suffering severe pathloss attenuation and channel particularities. As a consequence, conventional modulation schemes cannot fully benefit from the properties of the THz regime. In this context, novel modulation schemes, which take into account the channel particularities, have been presented in the open technical literature [8], [9]. In more detail, in [8], [9], the authors proposed the use of a time-spread on off keying (TSOOK) modulation scheme, which is about to countermeasure the impact of the THz channel. However, this modulation significantly restrains the achievable capacity, since the transmitted data "0" and "1" are mapped in silences and pulses. Moreover, it is applicable for very short transmission distances, e.g., in the order of mm, in which the impact of molecular absorption in the path loss is constrained.

In order to address this limitation, in [10] and [11], novel distance aware modulation schemes were presented, which permit adaptive transmissions of different symbols on non-overlapping and equally spaced sub-windows in parallel. Despite the fact that this scheme enables the utilization of longer-range links, due to the non-ovelapping nature of the sub-windows, the spectral efficiency loss may be important. Moreover, the implementation of non-continuous sub-windows is not an easy task for the transceivers [12], [13].

Motivated by this, this paper focuses on presenting a new distance and frequency dependent adaptive modulation scheme, which is suitable for multi-carrier communication systems operating in the THz band. After determining the transmission bandwidth, the proposed scheme evaluates the subcarrier bandwidth of the orthogonal frequency division modulated (OFDM) transmission signal, in order to countermeasure the frequency selectivity of the THz channel. Next, the power is allocated to the OFDM subcarriers and the modulation order of the quadrature modulated (QAM) symbol loaded in each subcarrier is selected, based on the instantaneous channel conditions and a predetermined bit error rate (BER) requirement. Our results, reveal that, by relaxing the BER requirement, data rates in the order of $\mathrm{Gb/s}$ can be achieved in transmission distances of 1 m.

II. System and Channel Model

In this section, we describe the system model and the THz channel characteristics. In more detail, in Section II-A, the signal model and the assumption of our analysis are provided, whereas, in Section II-B, the channel model for the 275–400 band is presented.

A. System Model And Network Topology

We consider a downlink transmission scenario in a wireless THz system, operating in time division duplex (TDD) mode, in which both the base station (BS) and user equipment (UE) are equipped with highly directive antennas and perform analog beamforming. Moreover, orthogonal frequency division multiplexing (OFDM), with $K+1$ subcarriers, is used in order to countermeasure the impact of frequency selectivity in the THz band. The fading channel of the link is assumed to be frequency selective and fixed, at least during a concurrent uplink and downlink transmissions. Both the BS and UE is assumed to have perfect channel state information (CSI), which is acquired, due to the channel reciprocity, without the use of a feedback channel.

The baseband equivalent received signal at the k-th subcarrier can be expressed as

$$r(k) = h(k)s(k) + n(k), \quad \text{with } k \in \left\{-\frac{K}{2}, \cdots, -1, 0, 1, \cdots, \frac{K}{2}\right\}, \tag{1}$$

where $s(k)$ denotes the transmitted quadrature amplitude modulated (QAM) symbol of M_k order on carrier k, whereas $h(k)$ and $n(k)$ respectively stand for the channel frequency response and additive white Gaussian noise (AWGN) component at the k-th subcarrier. Note that, it is assumed that the transmitted signal in subcarrier k was up-converted in the f_k frequency at the BS. Moreover, the order of the transmitted signal M_k will be selected based on the instantaneous channel quality and will guarantee that the error rate in the specific subcarrier will not surpass a predetermined threshold, while, at the same time, the maximum data rate will be achieved.

B. Channel Model

The channel coefficient, $h(k)$, is assumed to follow zero-mean complex Gaussian distribution, with variance that models the free space path and molecular absorption gains, i,e, the total path gain for the channel between the BS and UE, at frequency f_k, and can be evaluated as [3]

$$\sigma^2(f_k, d) = L_f(f_k, d)L_a(f_k, d), \tag{2}$$

where $L_f(f_k, d)$ and $L_a(f_k, d)$ respectively represents the free space and molecular absorption path gains at the frequency f_k, while d is the distance between the BS i and UE j.

The free space path gain can be evaluated, by radially expanding the wavefront adjusted with the BS and UE antenna gains, as

$$\mathrm{L_f}(f_k, d) = \frac{c^2}{(4\pi d f_k)^2} G_b(\Theta_i) G_u(\Theta_j), \tag{3}$$

where $G_b(\Theta_i)$ and $G_u(\Theta_j)$ represent the BS i and UE j antenna gain, respectively, and c is the speed of light. Note that the BS and UE antenna gains are usually dependent on the angles of incident Θ_i and reception Θ_j. By assuming that the TX and RX are aligned and analog pencil beamforming is employed, we can obtain that when the BS and UE antennas are aligned, $G_b(\Theta_i) = G_b$ and $G_u(\Theta_j) = G_u$.

On the other hand, the molecular absorption loss in the millimeter and THz frequency regions can be modeled according to the Beer-Lambert law as [9]

$$\tau(f_k, d) = \frac{P_u(f_k, d)}{P_b(f_k)} = e^{-\kappa_{\mathrm{a}}(f_k) d}, \tag{4}$$

where $\tau(f_k, d)$ stand for the transmittance, $P_b(f_k)$ represents the transmitted powers, and $\kappa_{\mathrm{a}}(f_k)$ denotes the absorption coefficient describing the relative absorbing area of the molecules in the medium per unit volume. The main cause of absorption loss in millimeter and THz frequencies is the water vapor that causes discrete, but deterministic loss to the signals in the frequency domain. Other molecules, such as oxygen, also cause some level of loss to the signals, but the water vapor dominates the overall molecular absorption loss above 200 GHz frequencies.

In order to evaluate the absorption loss, we utilize a simplified model for the molecular absorption loss in 275–400 GHz band, which was initially presented in [14]. According to this model, the molecular absorption gain can be estimated as

$$\mathrm{L_a}(f_k, d, \mu) = \exp(-d(y_1(f_k, \mu) + y_2(f_k, \mu) + g(f_k))), \tag{5}$$

where μ denotes the volume of the mixing ratio of water vapor. Note that the volume of the mixing ratio of water vapor is not equal to its relative humidity and it can be evaluated as

$$\mu = \frac{\phi}{100} \frac{p_w(T, p)}{p}, \tag{6}$$

where ϕ and p respectively stand for the relative humidity and the pressure, whereas $p_w(T, p)$ is the saturated water vapor partial pressure in temperature, T, measured in ^oC, and, according to Buck equation [15], can be calculated as

$$p_w(T, p) = w_1 \left(w_2 + w_3 p\right) \exp\left(\frac{w_4 T}{w_5 + T}\right), \tag{7}$$

where p is given in Pa, while $w_1 = 6.1121$, $w_2 = 1.0007$, $w_3 = 3.46 \times 10^{-8}$, $w_4 = 17.502$ and $w_5 = 240.97$. Moreover, the parameters $y_1(f_k, \mu)$, and $y_2(f_k, \mu)$, and $g(f_k)$ in (5) can be expressed as

$$y_1\left(f_k, \mu\right) = \frac{A(\mu)}{B(\mu) + \left(\frac{f_k}{100c} - c_1\right)^2}, \tag{8}$$

$$y_2\left(f_k, \mu\right) = \frac{C(\mu)}{D(\mu) + \left(\frac{f_k}{100c} - c_2\right)^2}, \tag{9}$$

and

$$g\left(f_k\right) = p_1 f_k^3 + p_2 f_k^2 + p_3 f_k + p_4, \tag{10}$$

where $c_1 = 10.835\ \mathrm{cm}^{-1}$, $c_2 = 12.664\ \mathrm{cm}^{-1}$, $p_1 = 5.54 \times 10^{-37}\ \mathrm{Hz}^{-3}$, $p_2 = -3.94 \times 10^{-25}\ \mathrm{Hz}^{-2}$, $p_3 = 9.06 \times 10^{-14}\ \mathrm{Hz}^{-1}$, $p_4 = -6.36 \times 10^{-3}$, and

$$A(\mu) = 0.2205\mu(0.1303\mu + 0.0294), \tag{11}$$

$$B(\mu) = (0.4093\mu + 0.0925)^2, \tag{12}$$

$$C(\mu) = 2.014\mu(0.1702\mu + 0.0303) \tag{13}$$

and

$$D(\mu) = (0.537\mu + 0.0956)^2. \tag{14}$$

This model was shown to have high accuracy for up to $1\ \mathrm{km}$ links in standard atmospheric conditions, i.e., temperature of $296\ ^{\mathrm{o}}\mathrm{K}$ and pressure of $101325\ \mathrm{Pa}$ [14]. Moreover, since the impact of the temperature and pressure can be modeled through the water vapor mixing ratio, μ, (5) can describe the THz link molecular absorption pathloss beyond the standard atmospheric conditions. Finally, note that the parameters c_1, c_2, p_1, p_2, p_3, and p_4 can be considered relatively independent of the atmospheric conditions [14].

Based on (2), (3), and (5), the total path gain can be rewritten as

$$\begin{aligned}\sigma^2\left(f_k, d\right) = &\frac{c^2}{(4\pi d f_k)^2} G_b G_u \\ &\times \exp\left(-d(y_1(f_k, \mu) + y_2(f_k, \mu) + g(f_k))\right).\end{aligned} \tag{15}$$

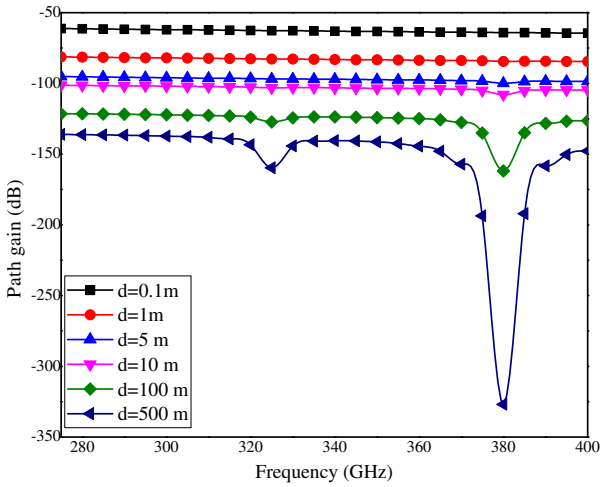

Fig. 1: Path gain variance as a function of the operation frequency for different transmission distances.

From (15), it is evident that the total path gain depends not only on the operation frequency and the distance between the BS and UE, but also on the BS and UE antenna gains, as well as the atmospheric conditions.

THz channel particularities: In order to reveal the THz channel particularities, in Fig. 1, we illustrate the path gain variance as a function of the frequency for different values of the BS-UE distance, assuming standard atmospheric conditions, and $G_b = G_u = 1$. From this figure, it is evident that as d increases, the frequency selectivity also increases; hence, the available communication bandwidth decreases.

III. The Proposed Link Adaptation Algorithm

As illustrated in Algorithn 1, given at the top of the page, the link adaptation mechanism consists of six steps. In the first step, the available transmission bandwidth is determined, $B(d)$, based on the channel selectivity in distance d. In more detail, according to [14, eq. (23)], the available transmission bandwidth can be obtained as

$$B(d) = f_c^h - \Delta f_h - \left(f_c^l + \Delta f_l\right), \tag{16}$$

where f_c^h and f_c^l represent the lower and higher absorption line center frequencies, respectively, and f_c is the center transmission frequency, whereas Δf_l and Δf_h can be obtained as

$$\Delta f_l = 100c\sqrt{\frac{1}{\frac{1}{\left(\frac{f_c}{100c} - b_1\right)^2 + b_2} + b_3\frac{\ln(\gamma)}{d\mu}} - b_2} \tag{17}$$

$$\Delta f_h = 100c\sqrt{\frac{1}{\frac{1}{\left(\frac{f_c}{100c} - g_1\right)^2 + g_2} + g_3\frac{\ln(\gamma)}{d\mu}} - g_2}, \tag{18}$$

where γ stands for the tolerance of the absorption loss deviation, whereas $b_1 = 10.842\ \text{cm}^{-1}$, $b_2 = 0.0098\ \text{cm}^{-2}$, $b_3 = 4.49 \times 10^3\pi$, $g_1 = 12.679\ \text{cm}^{-1}$, $g_2 = 0.0107\ \text{cm}^{-2}$, and $g_3 = 4.7 \times 10^2\pi$.

Algorithm 1 Algorithm for adaptive link adaptation

Input: d, μ, P_t, G_b, G_u, P_n, f_c, f_c^h, f_c^l, γ, ϵ, P_b
Output: N, $\mathbf{P}$, $\mathbf{M}$
Determine the maximum available bandwidth:
Calculate $B \leftarrow$ Eq. (16)
Determine the subcarrier bandwidth and number of subcarriers:
Calculate $\Delta f \leftarrow$ Eq. (19)
Calculate $N \leftarrow$ Eq. (20)
Calculate $L_{th} \leftarrow$ Eq. (21)
LOOP Process
for $k = -\frac{K}{2}$ to $\frac{K}{2}$ **do**
  Identify virtual subcarriers and allocate the transmission power:
  if $-20\log_{10}(h(k)) > L_{th}$ **then**
    Set $P(k) \leftarrow 0$,
    Set $\theta_k \leftarrow 0$
  else
    Calculate $P(k) \leftarrow$ Eq. (23)
    Set $\theta_k \leftarrow 1$
  end if
  Evaluate the achievable SNR and modulation order
  Calculate $\gamma_k \leftarrow$ Eq. (24)
  Calculate $M_k \leftarrow$ Eq. (27)
  if $M_k < 4$ **then**
    Set $M_k \leftarrow 2$,
  end if
end for
Set $\mathbf{P} \leftarrow \{P(k)\}_{k=-K/2}^{K/2}$
Set $\mathbf{M} \leftarrow \{M_k\}_{k=-K/2}^{K/2}$
Set $\theta \leftarrow \{\theta_k\}_{k=-K/2}^{K/2}$
return N, $\mathbf{P}$, $\mathbf{M}$, θ

Next, the bandwidth of the subcarrier, Δf, and the total number of subcarriers, $N = K + 1$, are selected, in a way that all the subcarriers to be frequency flat, i.e., they satisfy the following condition

$$|h(f + \Delta f) - h(f)|^2 \leq \epsilon. \tag{19}$$

Note that $B(d)$, Δf and N are connected through

$$N = \left\lfloor \frac{B(d)}{\Delta f} \right\rfloor, \tag{20}$$

where the operator $\lfloor x \rfloor$ returns the greatest integer less than or equal to x.

The objective of the third step is to identify virtual subcarriers, i.e., subcarriers that cannot support reliable symbol transmissions. As virtual subcarriers, we set the subcarriers in which the instantaneous pathloss is greater than a predetermined threshold, L_{th}, i.e., $-20\log_{10}(h(k)) > L_{th}$. By assuming that the total transmission power is uniformly

distributed in all of the subcarriers, the pathloss threshold can be calculated as

$$L_{th} = \frac{P_t}{N} + G_b + G_u - (\gamma_b + P_n), \tag{21}$$

where P_n represents the noise power at the k-th subcarrier at the receiver, whereas γ_b stands for the average signal-to-noise ratio (SNR), which is required in order to achieve a P_b^{BPSK} BER, when binary shift keying (BPSK) is employed, and it can be evaluated as

$$\gamma_b = \frac{\left(1 - 2P_b^{\text{BPSK}}\right)^2}{1 - \left(1 - 2P_b^{\text{BPSK}}\right)^2}. \tag{22}$$

In the forth step, the power is allocated to the non-virtual subcarriers, based on the water filling principal, as

$$P(k) = \begin{cases} C - \frac{P_n}{|h_k|^2} & \text{for } C > \frac{P_n}{|h_k|^2}, \\ 0, & \text{otherwise} \end{cases}, \tag{23}$$

where C is a constant whose value depends on the total transmitted power. Note that the water filling principle guarantees that the maximum capacity for a fixed total transmission power, P_t, can be achieved.

In the fifth step, the achievable SNR in each non-virtual subcarrier, k, is derived as

$$\gamma_k = \frac{|h_k|^2 P(k)}{P_n}. \tag{24}$$

In the final step, the modulation order, M_k, is selected in order to ensure a BER requirement, P_b. According to [16], the BER of M_k-QAM, with $M_k \geq 4$ can be obtained as

$$P_b = \frac{a}{2}\left(1 - \sqrt{\frac{\frac{3}{2}\frac{\gamma_k}{M_k - 1}}{1 + \frac{3}{2}\frac{\gamma_k}{M_k - 1}}}\right), \tag{25}$$

where

$$a = \begin{cases} 1, & \text{for } M_k = 4 \\ \frac{4}{\log_2(M_k)}, & \text{for } M_k > 4 \end{cases}. \tag{26}$$

From (25), the modulation order can be derived as the maximum power of 2 that satisfy the following condition

$$M_k \leq \frac{2\gamma_k}{3}\left(\frac{1}{\left(1 - \frac{2P_b}{a}\right)^2} - 1\right) + 1. \tag{27}$$

Note that if $M_k < 4$, the BPSK is employed.

IV. Results and Discussion

This section is devoted in presenting the impact of the input parameters on the algorithm performance, as well as evaluating its effectiveness, in terms of data rate, which can be derived as

$$R(d, P_b) = \Delta f \sum_{k=-K/2}^{K/2} \theta_k \log_2(M_k). \tag{28}$$

In what follows, it is assumed that the atmospheric pressure, relative humidity, and temperature are respectively 101325 Pa, 50%, and $23^o C$. The transmission power is set to 10 dBm, while the noise power equals -70 dBm. The antenna gains for both the TX and RX are 45 dB. Finally, in order to accommodate the multipath fading, we used the Saleh-Valenzuela channel model, whixh is proven to be appropriate for indoor THz communications [17]–[19].

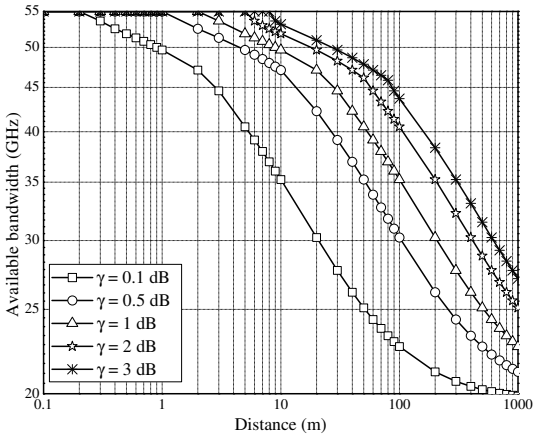

Fig. 2: Maximum available bandwidth as a function of the transmission distance, for different values of γ.

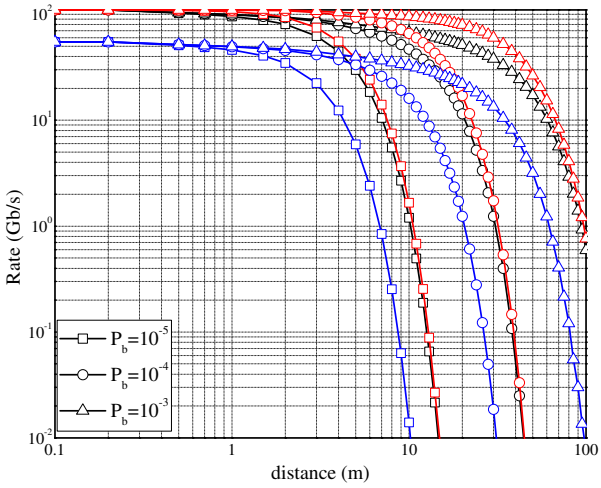

Fig. 3: Achievable data rate as a function of the transmission distance, for different values of P_b and $\gamma = 0.1$ dB (black colored lines), and $\gamma = 1$ dB (red colored lines).

In Fig. 2, the maximum available bandwidth is illustrated as a function of the transmission distance, for different values of γ, assuming standard atmospheric conditions. As expected, for a fixed γ, as the distance increases, the available bandwidth decreases. For instance, for $\gamma = 0.1$ dB, the available bandwidth decreases 35.72%, as the distance increases from 10 to 100 m. Moreover, for a fixed transmission distance, as γ increases, i.e., as the tolerance to the absorption loss relaxes, the available bandwidth also increases. For example, for $d = 10$ m, the available bandwidth increases 50.87%, as γ changes from 0.1 to 3 dB.

Fig. 3 depicts the achievable data rate as a function of the transmission distance, for different P_b and γ requirements. As

a benchmark, the corresponding achievable rate for the case in which, instead of the adaptive modulation scheme, BPSK is employed, and $\gamma = 0.1$ dB, is plotted (blue colored lines). As expected, for a given P_b and γ, as transmission distance increases, the available bandwidth decreases; hence, the data rate also decreases. For instance, for $P_b = 10^{-5}$ and $\gamma = 0.1$ dB, the data rate decreases from 100 Gb/s to 1.2 Gb/s, as the distance alters from 0.1 to 10 m. Moreover, for a given transmission distance and BER requirements, as γ increases, i.e., as the frequency flatness requirement relaxes, the available bandwidth and the number of subcarriers increases; therefore, the data rate also increases. Furthermore, for a fixed transmission distance and γ, as the BER requirement relaxes, the data rate increases. In other words, we observe that in order to achieve Gb/s data rates in 100 m transmission distances, the BER requirement should be in the order of 10^{-3}. Finally, from this figure, it is evident that the use of the adaptive modulation scheme plays an important role in improving the systems data rate and increasing the transmission distance. In particular, for $d = 10$ m and $P_b = 10^{-5}$, the use of the adaptive modulation scheme causes a 404.41% data rate increase.

V. Conclusions

In this paper, we presented a low-complexity distance and bandwidth dependent link adaptation algorithm, which is suitable for multi-carrier THz systems. By taking into account a predefined level of reliability and the distance between the BS and UE, the algorithm selects the available bandwidth and the modulation order that maximizes the data rate in each subcarrier, without violating the BER requirement. The results reveal the impact of BER requirement on the maximum achievable data rate in a specific transmission distance. Finally, we observed that the use of the link adaptation scheme contributes in increasing both the data rate and the transmission distance.

Acknowledgment

This work has received funding from the European Commission's Horizon 2020 research and innovation programme under grant agreement No. 761794.

References

[1] A.-A. A. Boulogeorgos, A. Alexiou, T. Merkle, C. Schubert, R. Elschner, A. Katsiotis, P. Stavrianos, D. Kritharidis, P.-K. Chartsias, J. Kokkoniemi, M. Juntti, J. Lehtomäki, A. Teixeira, and F. Rodrigues, "Terahertz technologies to deliver optical network quality of experience in wireless systems beyond 5G," *IEEE Commun. Mag.*, 2018.

[2] H. Shokri-Ghadikolaei, C. Fischione, G. Fodor, P. Popovski, and M. Zorzi, "Millimeter wave cellular networks: A MAC layer perspective," *IEEE Trans. Commun.*, vol. 63, no. 10, pp. 3437–3458, Oct. 2015.

[3] A.-A. A. Boulogeorgos, E. N. Papasotiriou, J. Kokkoniemi, J. Lehtomäki, A. Alexiou, and M. Juntti, "Performance evaluation of thz wireless systems operating in 275-400 ghz band," in *IEEE 87th Vehicular Technology Conference: International Workshop on THz Communication Technologies for Systems Beyond 5G*, Porto, Portugal, Jun. 2018.

[4] A.-A. A. Boulogeorgos, "Interference mitigation techniques in modern wireless communication systems," Ph.D. dissertation, Aristotle University of Thessaloniki, Thessaloniki, Greece, Sep. 2016.

[5] R. Piesiewicz, T. Kleine-Ostmann, N. Krumbholz, D. Mittleman, M. Koch, J. Schoebei, and T. Kurner, "Short-range ultra-broadband Terahertz communications: Concepts and perspectives," *IEEE Antennas. Propag.*, vol. 49, no. 6, pp. 24–39, Dec 2007.

[6] I. F. Akyildiz, J. M. Jornet, and C. Han, "Terahertz band: Next frontier for wireless communications," *Phys. Commun.*, vol. 12, pp. 16–32, Sep. 2014.

[7] C. Lin and G. Y. L. Li, "Terahertz communications: An array-of-subarrays solution," *IEEE Commun. Mag.*, vol. 54, no. 12, pp. 124–131, Dec. 2016.

[8] J. M. Jornet and I. F. Akyildiz, "Information capacity of pulse-based wireless nanosensor networks," in *8th Annual IEEE Communications Society Conference on Sensor, Mesh and Ad Hoc Communications and Networks*, Jun. 2011, pp. 80–88.

[9] ——, "Channel modeling and capacity analysis for electromagnetic nanonetworks in the terahertz band," *IEEE Trans. Wireless Commun.*, vol. 10, no. 10, pp. 3211–3221, Oct. 2011.

[10] C. Han and I. F. Akyildiz, "Distance-aware multi-carrier (DAMC) modulation in terahertz band communication," in *IEEE International Conference on Communications (ICC)*, Jun. 2014, pp. 5461–5467.

[11] ——, "Distance-aware bandwidth-adaptive resource allocation for wireless systems in the terahertz band," *IEEE Trans. Terahertz Sci. Technol.*, vol. 6, no. 4, pp. 541–553, Jul. 2016.

[12] G. D. Ntouni, A.-A. A. Boulogeorgos, D. S. Karas, T. A. Tsiftsis, F. Foukalas, V. M. Kapinas, and G. K. Karagiannidis, "Inter-band carrier aggregation in heterogeneous networks:design and assessment," in *Proc. International Symposium on Wireless Communications Systems (ISWCS)*, Barcelona, Spain, Aug. 2014.

[13] A.-A. A. Boulogeorgos, G. D. Ntouni, D. S. Karas, T. Tsiftsis, F. Foukalas, G. K. Karagiannidis, and C. Thomos, "MIMO link adaptation with carrier aggregation in LTE-A heterogeneous networks," in *European Conference on Networks and Communications (EuCNC)*, Jun. 2015, pp. 765–767.

[14] J. Kokkoniemi, J. Lehtomäki, and M. Juntti, "Simplified molecular absorption loss model for 275 – 400 gigahertz frequency band," in *Proc. European Conf. Antennas Propag.*, 2018, pp. 1–5.

[15] O. A. Alduchov and R. E. Eskridge, "Improved magnus form approximation of saturation vapor pressure," *J. Appl. Meteor.*, vol. 35, no. 4, pp. 601–609, Apr. 1996.

[16] A. Goldsmith, *Wireless Communications*. New York, NY, USA: Cambridge University Press, 2005.

[17] C. Lin and G. Y. Li, "Indoor Terahertz communications: How many antenna arrays are needed?" *IEEE Trans. Wireless Commun.*, vol. 14, no. 6, pp. 3097–3107, Jun. 2015.

[18] X. Gao, L. Dai, Y. Zhang, T. Xie, X. Dai, and Z. Wang, "Fast channel tracking for terahertz beamspace massive MIMO systems," *IEEE Trans. Veh. Technol.*, vol. 66, no. 7, pp. 5689–5696, Jul. 2017.

[19] S. Kim and A. Zajic, "Statistical modeling and simulation of short-range device-to-device communication channels at sub-THz frequencies," *IEEE Trans. Wireless Commun.*, vol. 15, no. 9, pp. 6423–6433, Sep. 2016.